Controllable Terahertz Cross-Shaped Three-Dimensional Graphene Intrinsically Chiral Metastructure and Its Biosensing Application

Somayyeh Asgari[1,2], Nosrat Granpayeh[1], and Tapio Fabritius[2]

[1]Center of Excellence in Electromagnetics, Optical Communication Laboratory, Faculty of Electrical Engineering, K. N. Toosi University of Technology, Tehran, Iran
[2]Information Technology and Electrical Engineering/OPEM, University of Oulu, Oulu, Finland

Abstract: In this research, a three-dimensional (3D) graphene intrinsically chiral metastructure in terahertz (THz) region was proposed and analyzed. The unit cell consists of bi-layer cross-shaped graphene ribbons in which the back layer is rotated compared to the front layer. Parameter retrieval method and Kramers-Kronig relations are used for theoretical analysis and derivation of the right-handed and left-handed electromagnetic effective refractive indices of the proposed structure. Based on our analysis, the proposed meta-structure has a tunable and controllable chiral response due to the tunability of graphene and circular dichroism (CD) was reached to 0.2. In order to evaluate the performance of the THz device in biosensor application, its characteristics in chiral biomolecule (collagen) sensing was analyzed. With an optimum design, our simulations show that the refractive index sensitivity value can be obtained as high as 0.96 THz per refractive index unit (THz/RIU) for the CD spectra. Proposed graphene chiral metastructure is promising enabler for controllable polarization-sensitive devices and systems such as tunable polarization filters, rotators, polarizers, biosensors, phase shifters, operating in the THz region.

Keywords: Graphene; Chiral; Metastructure; Terahertz devices; Effective electromagnetic parameters; Kramers-Kronig relations.

1. Introduction

Chiral metastructures are artificial materials with attractive properties [1, 2]. By careful design of the unit cells, chiral metastructures can manipulate the electromagnetic wave (EM) properties such as amplitude, phase [3], and polarization states [4]. Chiral metastructures have been exploited in applications including the polarization filters [5, 6], rotators [7, 8], polarizers [9, 10], sensors [11, 12], phase shifters [13, 14], and so on.

There are intrinsic and extrinsic chirality in structures. In intrinsically chiral structure, the object does not coincide with its mirror image. In extrinsically chiral structure, a nonchiral structure forms a geometrical arrangement with the incident wave that cannot be coincided with its mirror image and so the whole arrangement is chiral [15, 16].

Chiral metastructures are either three dimensional (3D) or two dimensional (2D) structures. 3D chirality leads to circular dichroism (CD) as a manifestation of optical activity while 2D chirality leads to circular conversion dichroism (CCD) as a manifestation of asymmetric transmission (AT) [17].

Experimental investigation of metastructures is challenging especially when the wavelength becomes shorter and that is why different theoretical models are very useful in metamaterial research and development. Parameter retrieval method [18] is a basic and important technique to obtain the effective electromagnetic properties of media, including metamaterials. Another useful approach for theoretical analysis is the Kramers-Kronig integrals which relate to the real and imaginary parts of the effective electromagnetic parameters. The effective electromagnetic refractive indices of the right-handed and left-handed circularly polarized (RCP and LCP respectively) waves of the proposed chiral structure derived by parameter retrieval method [18] and Kramers-Kronig relations [19].

Due to the unique properties of graphene, which is an arranged honeycomb lattice of single layer carbon atoms, has attracted noticeable attentions in photonics [20]. Nowadays, different kinds of mid-infrared (MIR) and THz graphene-based devices such as tunable filters [21, 22], polarizers [23, 24], absorbers [25-27], sensors [28, 29], logic gates [30, 31], antennas [32, 33], and demultiplexers [34, 35] are designed and proposed. Few planar single-layer type graphene chiral metamaterial structures which are composed of patterned single graphene layer have been proposed to achieve tunable two-dimensional chiral responses due to the tunability of graphene with lack of CD and weak chirality responses of CCD [36-38]. However, they are limited to 2D and have weak chirality. In addition, they do not explain what type of characteristics and possibilities can be obtained by more complex three-dimensional (3D) structures.

In this study, we proposed a 3D graphene intrinsically chiral metastructure composed of cross-shaped graphene patterns and analyzed its behavior in THz region. The transmission spectrum of the structure was analyzed under both

RCP and LCP incident waves. In addition, the tunability of transmission and circular dichroism (CD) was investigated. The parameter retrieval method and the Kramers-Kronig relations are used to derive the effective electromagnetic refractive indices of the proposed chiral structure. To promote the applicability of the proposed design, a THz biosensor to detect helical chiral biomolecules such as collagen was evaluated.

Control over CD spectra is very useful in the field of biosensing because many biomolecules such as DNA and protein are naturally chiral [39, 40]. The CD spectrum of our proposed device is tunable and controllable just by changing the external electrical bias voltage of graphene; without need to re-fabrication of the structure or the use of complex instruments such as pump laser. This is an important advantage compared to other proposed metal- or dielectric-based bi-layer chiral metastructures.

The remaining of this paper is organized as follows: In Section 2, the theoretical and simulation methods are presented. In Section 3, the simulation results are presented and discussed. Sensing application of the proposed structure is given in Section 4. Finally, the paper is concluded in Section 5.

2. Theoretical and Simulation Methods

The schematics of the periodic, unit cell, front, and back views of the proposed periodic 3D graphene intrinsically chiral metastructure are respectively shown in Figs. 1(a-d). The metastructure is composed of five layers: the front cross-shaped graphene pattern (Fig. 1(c)), the dielectric spacer, the back rotated cross-shaped graphene pattern (Fig. 1(d)), the dielectric, and the metal gold bar. The front patterned layer is rotated compared to the back one to achieve the chiral response. The proposed structure is optimized in CST full-wave Software package to get the best chirality response, CD, and best sensing platform. Geometrical parameters are obtained by use of the genetic algorithm optimization technique in CST. Genetic algorithms (GAs) are heuristic searches and optimization techniques inspired by natural evolution and known as a computational technique with potential applications in mathematical immunology [41]. Optimum parameters are given in Table 1.

Table 1. Optimum parameters of the proposed structure of Fig. 1.

Parameter	Value
Rotation angle of the front pattern to the x-axis (θ_f)	45°
Rotation angle of the back pattern to the x-axis (θ_b)	120°
Angle between the two rectangle strips of each graphene cross-shaped patterns (ψ)	40°
Length of rectangle graphene strips (L)	20 µm
Width of rectangle graphene strips (w)	5 µm
Thickness of the first dielectric spacer (d_1)	6 µm
Thickness of the second dielectric spacer (d_2)	6 µm
Unit cell dimension in x and y directions (P)	22 µm
Thickness of Alumina layers	50 nm
Thickness of Silicon layers	50 nm

Ultra-thin layers of alumina and silicon are only utilized for electrostatic biasing of graphene patterns and have negligible effects on responses at high frequencies [42]. Quartz with the refractive index of 1.96 [37] is used as the main dielectric substrate of the proposed structure. Two ports are placed in front and back of the proposed 3D graphene intrinsically chiral metastructure for excitation and detection of the RCP and LCP THz waves, respectively. The circularly polarized (CP) modes are defined with respect to +z axis. The CP modes of the two mentioned ports are adjusted with the electric field of $E_x = exp(-jkz)$, $E_y = exp(-jkz + ja)$, and E_z=0 (k denotes the wave vector, $a\epsilon(0, 2\pi)$ shows the phase of CP modes, and a=π/2 or 3π/2 corresponds respectively to LCP or RCP waves).

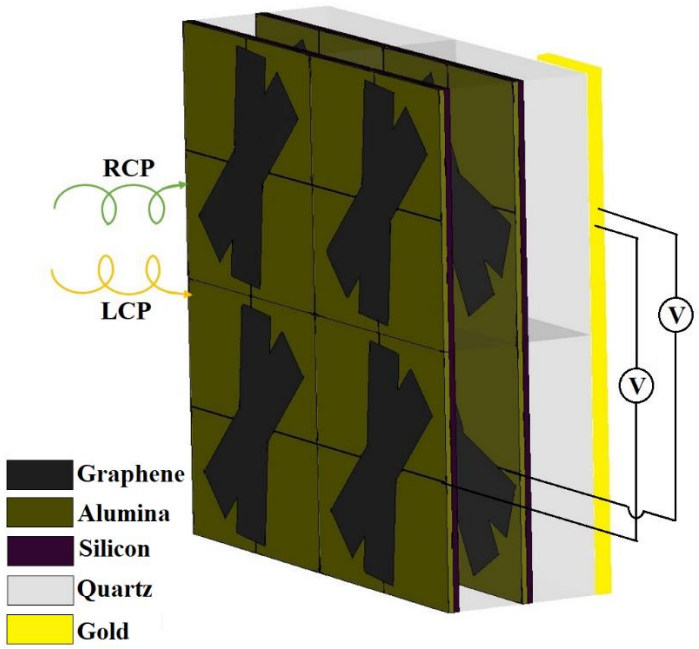

(a)

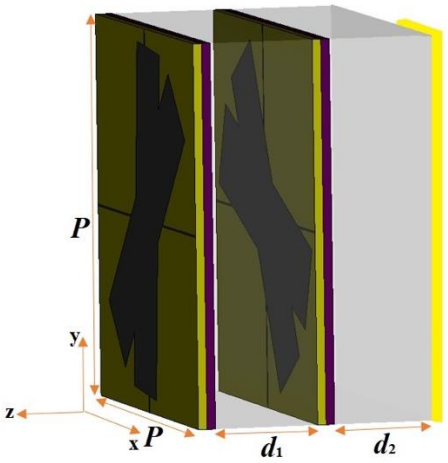

(b)

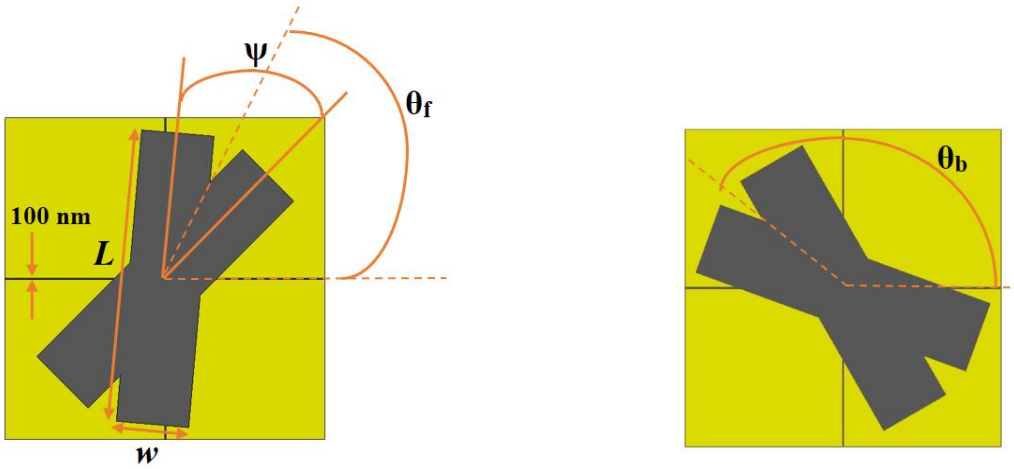

(c) (d)

Fig. 1. Schematics of the (a) periodic, (b) unit cell, (c) front, and (d) back views of the bi-layer 3D THz graphene chiral structure. Quartz dielectric is used as the main dielectric substrate between the front and back cross-shaped graphene patterns, and under the back-graphene cross-shaped pattern array. In addition, ultra-thin layers of alumina and silicon are utilized for electrostatic biasing of graphene.

The thickness of the graphene is assumed to be Δ=0.335 nm [43, 44]. The graphene relative permittivity is [45]:

$$\varepsilon = 1 - \frac{j\sigma_g}{\omega\varepsilon_0\Delta} \tag{1}$$

in which σ is the surface conductivity of the graphene and it is composed of the inter-band and intra-band electron transition contributions. σ and the electron transition contributions are as follows [46]:

$$\sigma_g = \sigma' + j\sigma'' = \sigma_{intra}(\omega) + \sigma_{inter}(\omega), \tag{2a}$$

in which σ_{intra} and σ_{inter} are [46]:

$$\sigma_{intra}(\omega) = \frac{2k_B e^2 T}{\pi\hbar^2} ln\left[2cosh\left(\frac{\mu_c}{2k_B T}\right)\right]\frac{j}{\omega + j\tau^{-1}}, \tag{2b}$$

$$\sigma_{inter}(\omega) = \frac{e^2}{4\hbar}\left[H\left(\frac{\omega}{2}\right) + \frac{4j\omega}{\pi}\int_0^\infty \frac{H(\zeta) - H\left(\frac{\omega}{2}\right)}{\omega^2 - 4\zeta^2} d\zeta\right], \tag{2c}$$

$$H(\zeta) = \frac{sinh\left(\frac{\hbar\zeta}{k_B T}\right)}{\left[cosh\left(\frac{\mu_c}{k_B T}\right) + cosh\left(\frac{\hbar\zeta}{k_B T}\right)\right]}. \tag{2d}$$

in which $\hbar = 1.054 \times 10^{-34}$ Js is the reduced Plank's constant, k_B=1.38×10^{-23} J/K is the Boltzmann's constant, e=1.6×10^{-19} C is the electron charge, and T=300 K. τ is the relaxation time calculated by [47]:

$$\tau = \frac{\mu_c \mu}{e v_f^2} \tag{3}$$

where v_f=10^6 m/s is the Fermi velocity and μ is the carrier mobility [48]. In the THz band, we have: $\hbar\omega \ll \mu_c$. So, the inter-band transition is neglected, and the intra-band transition is dominated [49].

The dispersion relation of the incident electromagnetic wave on the air-graphene-air can be expressed by [50]:

$$\beta = k_0\sqrt{1 - \left(\frac{2}{\eta_0\sigma_g}\right)^2} \tag{4}$$

where β, k_0, and η_0 are respectively the propagation constant of electromagnetic wave, the wave vector of incident light, and the impedance of air [50].

Thin graphene strips with the width of 100 nm, shown in Fig. 1(b), are considered to bias the cross-shaped graphene patterns electrically [26, 51]. The graphene chemical potential μ_c, of each layer could be controlled individually by the applied external bias voltage. The relation between μ_c and the applied bias voltage can be expressed as [52-54]:

$$|\mu_c(V)| = \hbar v_f\sqrt{\pi|a_0(V - V_0)|}; \tag{5}$$

where V_0 is the offset voltage [53], $a_0 = \frac{\varepsilon_0 \varepsilon_d}{ed}$ in which a_0 is the capacitive model of the structure, ε_0 is the vacuum permittivity, ε_d is the dielectric permittivity, d (d_1=d_2=6 μm) is the thickness of the dielectric, V is the external applied bias voltage to graphene layers (shown in Figs. 1(a) and 1(b)).

The chirality response of the proposed structure, circular dichroism (CD), is defined as the differential of the RCP and LCP absorption spectra, $A_R = 1 - |\tau_R|^2 - |r_R|^2$ and $A_L = 1 - |\tau_L|^2 - |r_L|^2$where τ_R, τ_L, and r_R, r_L are respectively the transmission and reflection coefficients of RCP and LCP waves [55, 56]:

$$CD = A_L - A_R \tag{6}$$

Since there is a relation between transmission and absorption, some works such as [55] reported their CD spectra based on the differences in transmissions.

By assumption of the incident electromagnetic wave as $e^{j\omega t}$, related to the incident angular frequency of ω, the constitutive relations for an isotropic chiral medium can be written as [57]:

$$\boldsymbol{D} = \varepsilon_r \varepsilon_0 \boldsymbol{E} - j\frac{\kappa}{c}\boldsymbol{H} \tag{7}$$

$$\boldsymbol{B} = j\frac{\kappa}{c}\boldsymbol{E} + \mu_r \mu_0 \boldsymbol{H} \tag{8}$$

where **D**, **E**, **B**, and **H** are respectively the electric and magnetic flux densities and fields. Also, ε_0, μ_0, ε_r, μ_r, c, and κ are respectively the permittivity and permeability of vacuum, the relative permittivity and relative permeability of the chiral medium, the speed of light in vacuum, and the chirality parameter. By using Maxwell's equations and doing some algebra, the wave equation of a chiral medium can be written as [57]:

$$\nabla^2 \boldsymbol{E} + 2\frac{\kappa\omega}{c}\nabla \times \boldsymbol{E} + \frac{\omega^2}{c^2}(\mu_r \varepsilon_r - \kappa^2)\boldsymbol{E} = 0 \tag{9}$$

So, the eigenmode of the electromagnetic wave equation of the chiral medium is only the RCP or LCP wave. In this regard, the fields split into two uncoupled CP waves. Although, the proposed THz complex structure is an anisotropic medium, each of the CP waves sees the chiral medium as an equivalent isotropic medium [57].

The effective electromagnetic refractive indices of the chiral media could be derived by use of the parameter retrieval method [18] and the Kramers-Kronig relations [19]. In the parameter retrieval method, by deriving electric and magnetic fields for a chiral slab, and applying the boundary conditions of continuity of tangential electric and magnetic fields at the both surfaces of the chiral slab and doing some manipulations, we get [18]:

$$\tau_{R,L} = \frac{4Ze^{jnk_0 d_1} e^{\pm \kappa k_0 d_1}}{(1+Z)^2 - (1-Z)^2 e^{2jnk_0 d_1}} \tag{10}$$

$$r_{R,L} = \frac{(1-Z^2)(e^{2jnk_0 d_1} - 1)}{(1+Z)^2 - (1-Z)^2 e^{2jnk_0 d_1}} \tag{11}$$

where Z, n, k_0, and d_1 are respectively the impedance of the chiral structure, refractive index of the chiral structure, vacuum wavenumber, and the thickness of the spacer between the front and back graphene patterns. The optical path of incident RCP or LCP wave in forward direction is $n_R d_1$ or $n_L d_1$. For the reflected wave in the backward direction, the optical path is $n_L d_1$ or $n_R d_1$). Therefore, the total optical paths for RCP and LCP waves are $(n_R + n_L)d_1$. Based on the Eq. 11 we can state that $r_R = r_L = r$. As the optical paths in forward direction are different for RCP and LCP waves, $\tau_R \neq \tau_L$ and thus $A_R \neq A_L$.

The refractive indices of RCP and LCP waves $n_{R,L}$, and the chirality parameter κ, for a time harmonic field of $e^{j\omega t}$ could be respectively obtained by [18]:

$$n_{R,L} = \frac{j}{k_0 d_1}\left\{ln\left[\frac{1}{\tau_{R,L}}\left(1 - \frac{Z-1}{Z+1}r\right)\right]\right\} \tag{12}$$

$$\kappa = \frac{j}{2k_0 d_1} ln\left(\frac{\tau_R}{\tau_L}\right) \tag{13}$$

Because of the multibranch form of complex logarithmic function, Eq. (12) ambiguously gives the real and the imaginary parts of $n_{R,L}$ as follows:

$$Re\{n_{R,L}\} = \frac{-1}{k_0 d_1} Im\left\{ln\left[\frac{1}{\tau_{R,L}}\left(1 - \frac{Z-1}{Z+1}r\right)\right]\right\} + \frac{2m\pi}{k_0 d_1} \tag{14a}$$

$$Im\{n_{R,L}\} = \frac{1}{k_0 d_1} Re\left\{ln\left[\frac{1}{\tau_{R,L}}\left(1 - \frac{Z-1}{Z+1} r\right)\right]\right\} \tag{14b}$$

where *m* is an integer determined by the branches of the ln function, respectively. *Z* is obtained by:

$$Z = \pm\sqrt{\frac{(1+r)^2 - \tau_R \tau_L}{(1-r)^2 - \tau_R \tau_L}} \tag{15}$$

The resulting uncertainty due to the existence of *m* in Eq. (14a), is referred as a branching problem, which affects only the real part of the refractive indices. The imaginary part of these parameters can be unambiguously determined using Eq. (14b). Considering this fact, K-K relations which connect the real and imaginary parts of the material parameters based on the causality principle are applied for solving the branch selecting problem in Eq. (14a).

In addition, the effective parameters of the chiral metastructure could be derived by use of Kramers-Kronig relations as follows [19]:

$$\mathrm{Re}\{a(\omega)\} = \mathrm{Re}\{a(\infty)\} + \frac{2}{\pi} P \cdot V. \int_0^\infty \frac{u\,\mathrm{Im}\{a(u)\}}{u^2 - \omega^2} du \tag{16}$$

and

$$\mathrm{Im}\{a(\omega)\} = -\frac{2\omega}{\pi} P \cdot V. \int_0^\infty \frac{\mathrm{Re}\{a(u)\} - \mathrm{Re}\{a(\infty)\}}{u^2 - \omega^2} du \tag{17}$$

where ω, *P.V.*, $a(\omega)$, and u respectively refer to the wave angular frequency, the principle value of the integral, one of the electromagnetic effective parameters of the chiral metastructure, and variable which the Integral is calculated based on it. By insertion of $n(\omega)$ in Eq. (16), we have:

$$\mathrm{Re}\{n(\omega)\} = \mathrm{Re}\{n(\infty)\} + \frac{2}{\pi} P \cdot V. \int_0^\infty \frac{u\,\mathrm{Im}\{n(u)\}}{u^2 - \omega^2} du \tag{18}$$

We also have [18]:

$$n_{R,L} = n \pm \kappa \tag{19}$$

By using Eqs. 12-19, the real part of the $n_{R,L}$ could be calculated by use of its imaginary part as follows [19]:

$$\mathrm{Re}\{n_{R,L}(\omega)\} = 1 + \frac{2}{\pi} P \cdot V. \int_0^\infty \frac{u\,\mathrm{Im}\{n_{R,L}(u) \mp \kappa(u)\}}{u^2 - \omega^2} du \pm \frac{2\omega}{\pi} P \cdot V. \int_0^\infty \frac{\mathrm{Im}\{\kappa(u)\}}{u^2 - \omega^2} du \tag{20}$$

3. Results and discussion

CST microwave studio as a full wave simulation Software is used to analyze the transmission spectra of our proposed structure. Absorbing boundary condition is used along the z-direction and periodic boundary conditions are applied to the x and y directions.

Due to the chiral nature (asymmetric geometry and lack of mirror symmetry) of the proposed metastructure shown in Fig. 1, transmission and absorption spectra for RCP and LCP waves would be different (τ_R and τ_L, as a result A_R and A_L, are not equal in the resonance frequencies; $\tau_R \neq \tau_L$ in chiral metastructures; Eq. (19)) causing differences in the resonance frequency, resonance intensity and CD. The simulated reflection and transmission, and absorption (for RCP, and LCP) spectra of the meta-structure depicted in Fig. 1 are respectively shown in Figs. 2(a) and 2(b).

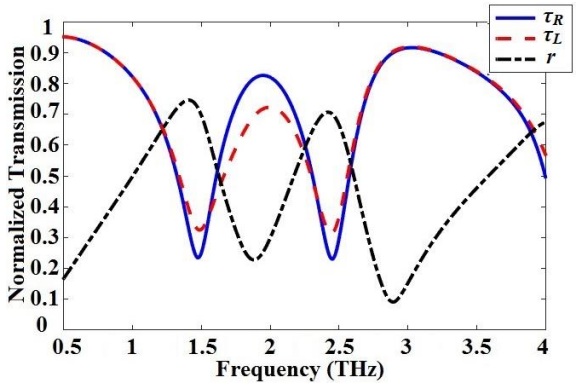

(a)

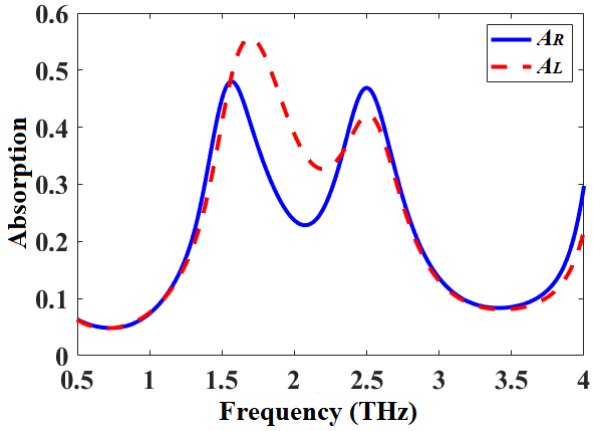

(b)

Fig. 2. (a) Reflection and RCP and LCP transmission, and (b) absorption spectra of the proposed structure of Fig. 1.

The observed chiral asymmetry in transmission and absorption spectra in Figs. 2(a) and 2(b) can also be demonstrated by showing the electric field distributions. Figures 3(a-h) display the electric field distributions of the proposed bi-layer graphene chiral structure of Fig. 1 under RCP and LCP incident lightwaves at the two resonance frequencies of 1.48 and 2.46 THz. The distributions show a clear dependence on the polarization of the incident light, resulting in differences in the normalized transmission and absorption spectra of RCP and LCP lightwaves (τ_R and τ_L, as a result A_R and A_L, are not equal in the resonance frequencies; $\tau_R \neq \tau_L$ in chiral metastructures, as depicted in Eq. (10)). For example, as shown in Figs. 3(a) and 3(b), the front layer does not have equal distributions for RCP and LCP normal incident illuminations which is obvious that the chiral nature (asymmetric geometry and lack of mirror symmetry) of the proposed structure of Fig. 1 causes these differences (the same as the electric field distributions in Figs. 3(c-h)).

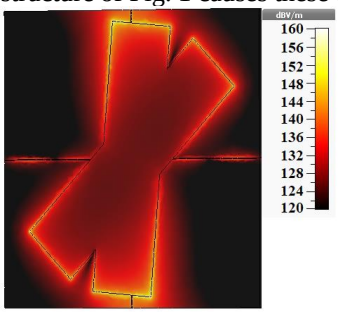

(a)

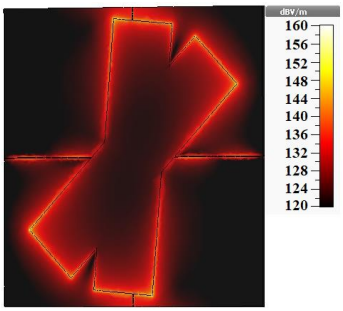

(b)

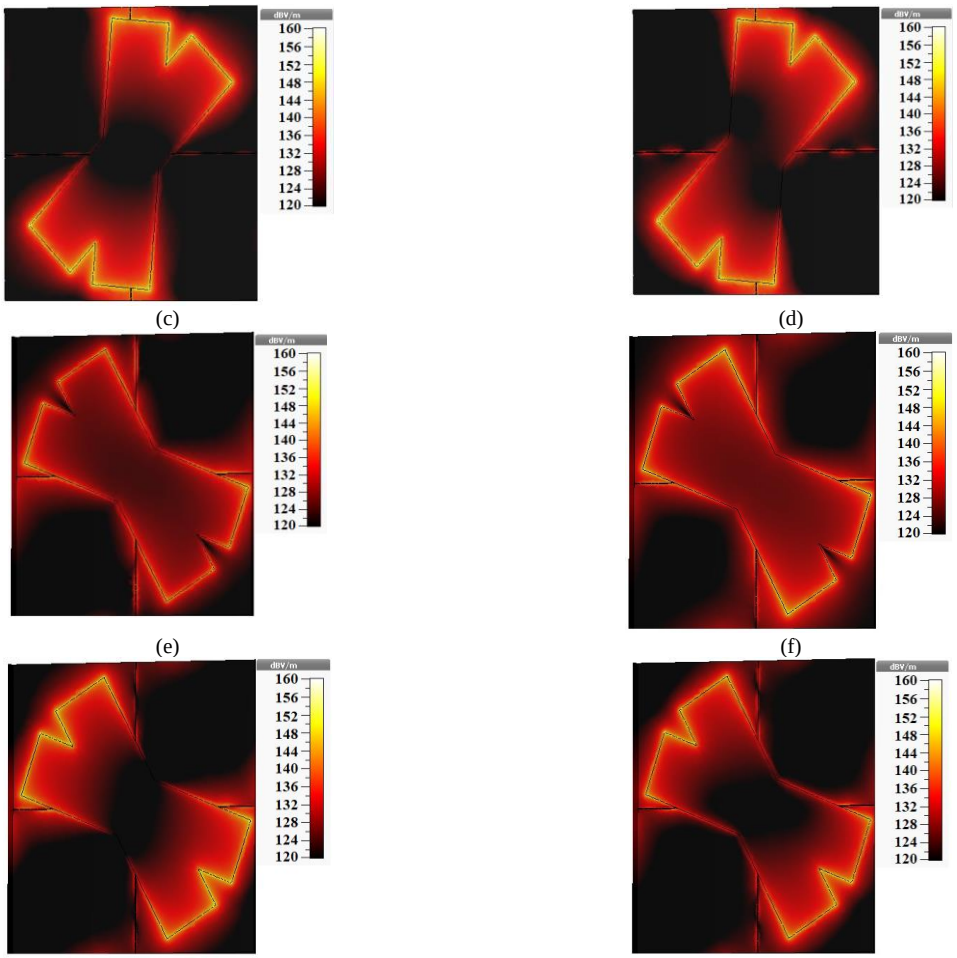

Fig. 3. Electric field distributions of the proposed bi-layer graphene chiral structure of Fig. 1 for the front layer for (a) RCP in 1.48 THz, (b) LCP in 1.48 THz, (c) RCP in 2.46 THz, (d) LCP in 2.46 THz; for the back layer for (e) RCP in 1.48 THz, (f) LCP in 1.48 THz, (g) RCP in 2.46 THz, (h) LCP in 2.46 THz.

The real part of β is related to the σ_g (Eq. 4) and σ_g is related to the μ_c (Eq. 2). As the μ_c increases, the real part of the β decreases (depicted in Fig. 4(a)) [58, 59]. The frequency of the CD peak should thus exhibit a blue shift when the μ_c increases. This shows that how the CD spectrum can be tuned by the change of the μ_c of graphene. CD of the proposed structure for four different chemical potentials of graphene are illustrated in Fig. 4(b). As a noticeable consequence, CD spectrum of the proposed chiral structure is tunable by change of the applied bias voltage of graphene without need to re-fabricate the structure or need of any other extra complex instruments such as pump laser and so on which are needed and used for the 3D type bi-layer metal- or dielectric-based chiral metastructures.

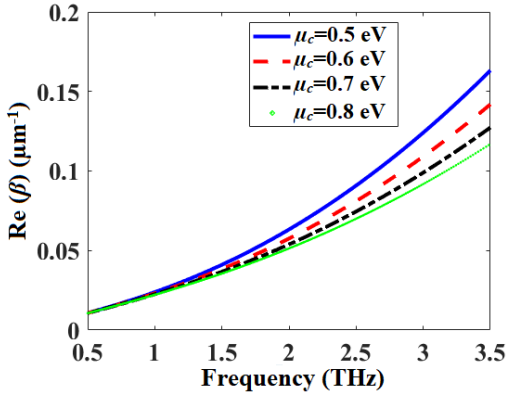

(a)

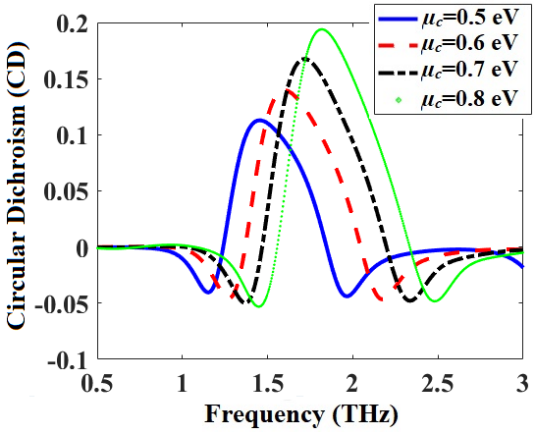

(b)

Fig. 4. (a) The real part of β (Eq. 4) of the graphene layer and (b). Circular dichroism (CD) of the proposed structure of Fig. 1 for different chemical potentials of graphene.

The imaginary parts of the n_R and n_L are calculated by Eq. 14b. The real parts of n_R and n_L are calculated by Eq. 20 by assumption of m=0. The obtained results are depicted in Figs. 5(a) and 5(b). Both methods show similar characteristics for m=0 over the whole frequency range of 0.5-4 THz.

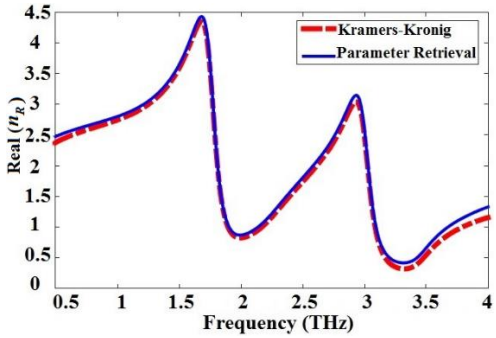

(a)

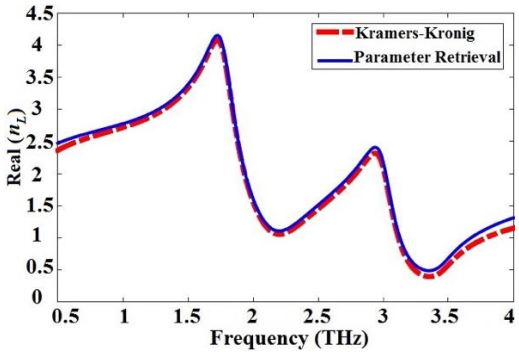

(b)

Fig. 5. (a) The real parts of the (a) n_R and (b) n_L calculated by Eqs. 19 and 20 theoretically.

4. Sensing Application

As an application of the proposed controllable graphene chiral structure, a refractive index- and a biosensor is designed and optimized in THz region which would become a useful THz structure in chiral biomolecular sensing. Schematic view of the unit cell of the bi-layer 3D THz graphene chiral sensor is given in Fig. 6(a). The analyte is placed over the sensor structure for investigation as shown in Fig. 6(a). By optimization of the proposed sensor device of Fig. 1, we realized that the maximum sensitivity of the proposed structure would be achievable when μ_c=0.5 eV. But, for μ_c=0.5 eV, we have minimum CD (Fig. 4(b)). By a tradeoff between CD and sensitivity, the optimum value of μ_c is chosen as 0.65 eV for the proposed sensor design. Other optimum parameters for gaining the maximum sensitivity are the same as reported in Table 1. Simulations reveal that the refractive index sensitivity value ($SS = \frac{\Delta f}{\Delta n}$: the rate of variation of the resonance frequency with respect to analyte refractive index, in terahertz per refractive index unit (THz/RIU).) can be obtained as high as 0.96 (THz/RIU) for the CD spectra. CD spectra of the sensor device for different refractive indices of the analyte are illustrated in Fig. 6(b).

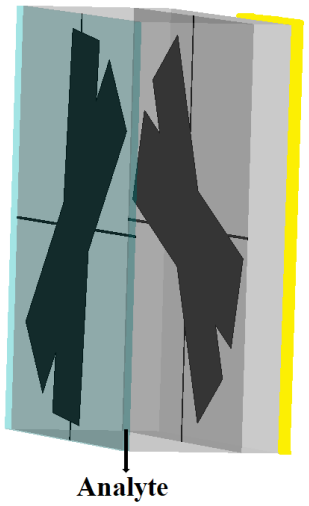

(a)

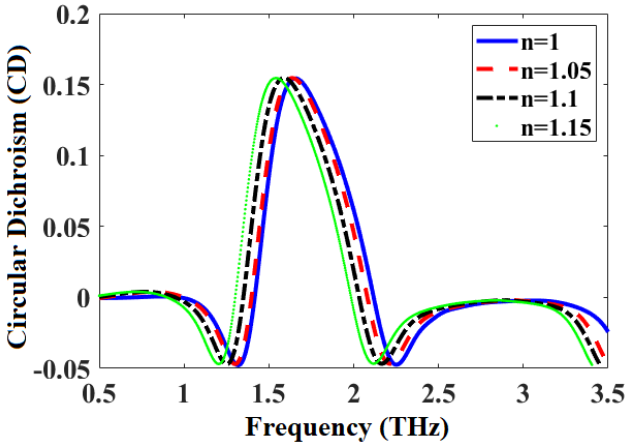

(b)

Fig. 6. (a) Schematic view of the unit cell of the bi-layer 3D THz graphene chiral sensor. (b) CD spectra of the sensor for different refractive indices of the analyte.

The interaction of proposed THz meta-structure with helical chiral biomolecules, collagen in this case, were evaluated by modeling to promote the applicability of developed structure for biosensing. It is worth to mention, that proposed structure can be utilized also as a refractive index micro sensor in THz region which is expected to have a noticeable high sensitivity to detect the materials.

The permittivity of collagen biomolecule is calculated by the Debye model [60]:

$$\varepsilon = \varepsilon_{\infty} + \frac{\Delta\varepsilon_1}{1+j\omega\tau_1} + \frac{\Delta\varepsilon_2}{1+j\omega\tau_2} \tag{21}$$

where ε_{∞}, $\Delta\varepsilon_1$, $\Delta\varepsilon_2$, ω, τ_1, and τ_2 are respectively the permittivity at infinite frequency, the difference between the static permittivity and the permittivity at the first and the second frequencies; the angular frequency, and the relaxation time of the first and the second frequencies. The optical properties of collagen by use of double Debye model in THz region are extracted in [60]. Table 2 shows the optical parameters of the double Debye model for collagen at the THz frequency region [60].

Table 2. Parameters of the double Debye model for Collagen helical biomolecule in THz region [60].

ε_{∞}	$\Delta\varepsilon_1$	τ_1 (ps)	$\Delta\varepsilon_2$	τ_2 (ps)
1.63	500	17.7	100	3.64

The proposed graphene chiral structure is covered by a layer of collagen helical biomolecules with thickness of 1.5 nm and illuminated by normal incident lightwave. The CD spectra of the proposed structure are obtained for the two cases with and without the collagen layer. As shown in Fig. 7, when the collagen layer is placed on the structure, the resonance frequency of the CD varies. So, the structure could be used as a biosensor for detection of chiral biomolecules in THz region. It is an advantage that the CD spectra of the proposed chiral metastructure are dynamically controllable by change of μ_c which is not possible by other metal- or dielectric-based chiral metastructures.

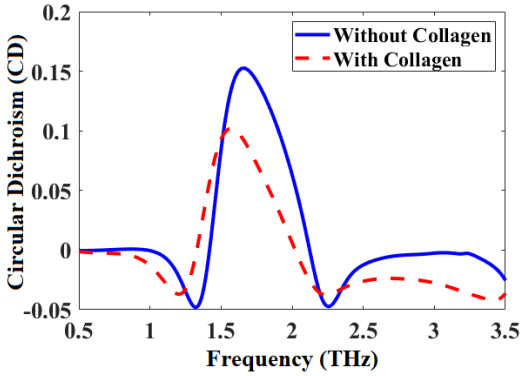

Fig. 7. CD spectra of the THz biosensor with and without Collagen considered on the structure of Fig. 1.

Sensitivity, tunability, and material type of our proposed sensor with some other works in THz frequency range are compared in Table 3.

Table 3. Sensitivity, tunability, and material type comparison of our proposed sensor with some other works in THz frequency range.

Ref.	[61]	[62]	[63]	[64]	[65]	[66]	[67]	[68]	Our work
SS (THz/RIU)	0.085	0.091	0.037	0.023	0.08	0.075	0.744	0.066	0.96
Tunability	no	no	no	no	no	no	yes	yes	yes
Material type	metal	metal	metal	dielectric	metal	metal	graphene	graphene	graphene

Fabrication of our proposed cross-shaped graphene chiral metastructure would be possible in THz region by use of direct laser writing of the graphene patterns on the substrate [69]. Then, the bi-layer chiral meta-device would be available by stacking up of the layers [70]. Fabrication technology of the proposed polarization-sensitive THz device needs further investigation and would be studied in future works.

5. Conclusion

In this work, we have proposed and analyzed a bi-layer three-dimensional (3D) graphene intrinsically chiral metastructure composed of cross-shaped graphene patterns in terahertz (THz) region. The back cross-shaped patterned graphene layer is rotated compared to the front one. The parameter retrieval method and the Kramers-Kronig relations are used for derivation of the effective refractive indices of the RCP and LCP waves of the proposed intrinsically chiral metastructure. Chiral response, the circular dichroism (CD), of the structure is tunable and controllable due to the tunability of graphenes by applying of the external bias voltage which is reached to 0.2. A refractive index- and a biosensor with controllable CD as an application of the proposed device for detection of chiral biomolecules is proposed and analyzed in THz region. With an optimum design, our simulations show that the refractive index sensitivity value can be obtained as high as 0.96 THz per refractive index unit (THz/RIU) for the CD spectra. The proposed structure is a useful segment in developing of dynamically controllable chiral devices and structures in THz region.

Acknowledgement

This work was supported in part by the Academy of Finland's Finnish Research Infrastructures (FIRI) under Grant 320017.

References

[1] E. Philip, M. Z. Güngördü, S. Pal, P. Kung, and S. M. Kim, "Review on Polarization Selective Terahertz Metamaterials: from Chiral Metamaterials to Stereometamaterials," J. Infrared Milli. Terahz. Waves Vol. 38, pp. 1047-1066, 2017.
[2] D. B. Stojanović, P. P. Beličev, J. Radovanović, and V. Milanović, "Numerical parametric study of chiral effects and group delays in Ω element based terahertz metamaterial," Phys. Lett. A, Vol. 383, pp. 1816-1820, 2019.

[3] S. Han, H. Yang, L. Guo, X. Huang, and B. Xiao, "Manipulating linearly polarized electromagnetic waves using the asymmetric transmission effect of planar chiral metamaterials," J. Opt. Vol. 16, pp. 035105, 2014.
[4] K. Chen, Y. Feng, L. Cui, J. Zhao, T. Jiang, and B. Zhu, "Dynamic control of asymmetric electromagnetic wave transmission by active chiral metamaterial," Sci. Rep. Vol. 7, pp. 42802, 2017.

[5] N. Yogesh, T. Fu, F. Lan, and Z. Ouyang, "Far-Infrared Circular Polarization and Polarization Filtering Based on Fermat's Spiral Chiral Metamaterial," IEEE Photon. J. Vol. 7, pp. 4600212, 2015.

[6] A. Basiri, X. Chen, J. Bai, P. Amrollahi, J. Carpenter, Z. Holman, C. Wang, and Y. Yao, "Nature-inspired chiral metasurfaces for circular polarization detection and full-Stokes polarimetric measurements," Light Sci. Appl. Vol. 78, pp. 1-11, 2019.

[7] J. Zhao and Y. Cheng, "Ultrathin dual-band polarization angle independent 90° polarization rotator with giant optical activity based on planar chiral metamaterial," Appl. Phys. B, Vol. 124, pp. 185 (1-7), 2018.

[8] K. Song, X.P. Zhao, Q.H. Fu, Y.H. Liu, and W.R. Zhu, "Wide-angle 90°-polarization rotator using chiral metamaterial with negative refractive index," Journal of Electromagnetic Waves and Applications, Vol. 26, pp. 1967-1976, 2012.
[9] J. Wang, Z. Shen, and W. Wu, "Broadband and high-efficiency circular polarizer based on planar-helix chiral metamaterials," Appl. Phys. Lett. Vol. 111, pp. 113503, 2017.

[10] S.-E. Mun, J. Hong, J.-G. Yun, and B. Lee, "Broadband circular polarizer for randomly polarized light in few-layer metasurface," Sci. Rep. Vol. 9, pp. 2543, 2019.

[11] S. Yoo and Q-H. Park, "Metamaterials and chiral sensing: a review of fundamentals and applications," Nanophononics, Vol. 8, pp. 249-261, 2019.

[12] Ş. Dalgaç, M. Bakır, F. Karadağ, E. Ünal, M. Karaaslan, and C. Sabah, "Characterization of chiral metamaterial sensor with high sensitivity," Optik, 2019, https://doi.org/10.1016/j.ijleo.2019.163673.

[13] Z. Yang, Z. Wang, H. Tao, and M. Zhao, "Manipulation of wavefront using helical metamaterials," Opt. Express, Vol. 24, pp. 18266-18276, 2016.

[14] Z. Ma, Y. Li, Y. Li, Y. Gong, S. A. Maier, and M. Hong, "All-dielectric planar chiral metasurface with gradient geometric phase," Opt. Express, Vol. 26, pp. 6067-6078, 2018.

[15] E. Plum, V. A. Fedotov and N. I. Zheludev, "Extrinsic electromagnetic chirality in metamaterials," J. Opt. A: Pure Appl. Opt. Vol. 11, pp. 074009, 2009.

[16] E. Plum, V. A. Fedotov and N. I. Zheludev, "Optical activity in extrinsically chiral metamaterial," Appl. Phys. Lett. Vol. 93, pp. 191911, 2008.

[17] L. Wu, Z.Y. Yang, Y.Z. Cheng, Z.Q. Lu, P. Zhang, M. Zhao, R.Z. Gong, X.H. Yuan, Y. Zheng, and J.A. Duan, "Electromagnetic manifestation of chirality in layer-by-layer chiral metamaterials," Opt. Express Vol. 21, pp. 5239–5246, 2013.

[18] R. Zhao, T. Koschny, and C. M. Soukoulis, "Chiral metamaterials: retrieval of the effective parameters with and without substrate," Opt. Express, Vol. 18, pp. 14553-14567, 2010.

[19] V. Lucarini, K. E. Peiponen, J. J. Saarinen, and E. M. Vartiainen, *Kramers-Kronig Relations in Optical Materials Research*, 2005.

[20] F. Bonaccorso, Z. Sun, T. Hasan, and A. C. Ferrari, "Graphene photonics and optoelectronics," Nat. Photonics, Vol. 4, pp. 611-622, 2010.

[21] S. Li, W. Chen, P. Wang, Q. Fu, J. Zhang, B. Zhang, T. Dai, Y. Wang, and J. Yang, "Bandwidth-tunable optical passband filter based on graphene–silicon waveguide," Opt. Commun. Vol. 426, pp. 206-211, 2018.

[22] S. Asgari, H. Rajabloo, N. Granpayeh, and H. Oraizi, "Tunable graphene-based mid-infrared band-pass planar filter and its application," Chin. Phys. B, Vol. 27, pp. 084212, 2018.

[23] Yu. V. Bludova, M. I. Vasilevskiy, and N. M. R. Peres, "Tunable graphene-based polarizer," J. Appl. Phys. Vol. 112, pp. 084320 (1-5), 2012.

[24] X. He and J. Liu, “Flexible and broadband graphene polarizer based on surface silicon-core microfiber,” Opt. Mater. Express, Vol. 7, pp. 1398-1405, 2017.

[25] S. Biabanifard, M. Biabanifard, S. Asgari, S. Asadi, and C. E. Mustapha, “Tunable ultra-wideband terahertz absorber based on graphene disks and ribbons,” Opt. Commun. Vol. 427, pp. 418-425, 2018.

[26] M. Biabanifard, S. Asgari, S. Biabanifard, and M. S. Abrishamian, “Analytical design of tunable multi-band terahertz absorber composed of graphene disks,” Optik, Vol. 182, pp. 433-442, 2019.

[27] M. Huang, Y. Cheng, Z. Cheng, H. Chen, X. Mao, and R. Gong, “Based on graphene tunable dual-band terahertz metamaterial absorber with wide-angle,” Opt. Commun. Vol. 415, pp. 194-201, 2018.

[28] S. Asgari and N. Granpayeh, “Tunable Mid-Infrared Refractive Index Sensor Composed of Asymmetric Double Graphene Layers,” IEEE Sens. J. Vol. 19, pp. 5686 - 5691, 2019.

[29] C. Liang, G. Niu, X. Chen, Z. Zhou, Z. Yi, X. Ye, T. Duan, Y. Yi, and S. Xiao, “Tunable triple-band graphene refractive index sensor with good angle-polarization tolerance,” Opt. Commun. Vol. 436, pp. 57-62, 2019.

[30] S. Asgari and N. Granpayeh, “Applications of tunable nanoscale midinfrared graphene based slot cavity in nanophotonic integrated circuits,” IEEE Trans. Nanotechnol. Vol. 17, pp. 533-542, 2018.

[31] S. Asgari, N. Granpayeh, and Z. G. Kashani, “Plasmonic mid-infrared wavelength selector and linear logic gates based on graphene cylindrical resonator,” IEEE Trans. Nanotechnol. Vol. 18, pp. 42-50, 2019.

[32] A. Scidà, S. Haque, E. Treossi, A. Robinson, S. Smerzi, S. Ravesi, S. Borini, and V. Palermo, “Application of graphene-based flexible antennas in consumer electronic devices,” Mater. Today, Vol. 21, pp. 223-230, 2018.

[33] Y. Wan, Y. An, Z. Tao, and L. Deng, “Manipulation of surface plasmon resonance of a graphene-based Au aperture antenna in visible and near-infrared regions,” Opt. Commun. Vol. 410, pp. 733-739, 2018.

[34] S. Asgari and N. Granpayeh, “Tunable plasmonic dual wavelength multi/demultiplexer based on graphene sheets and cylindrical resonator,” Opt. Commun. Vol. 393, pp. 5-10, 2017.

[35] S Asgari and T Fabritius, “Tunable Mid-Infrared Graphene Plasmonic Cross-Shaped Resonator for Demultiplexing Application,” Appl. Sci. Vol. 10, pp. 1193, 2020.

[36] T. Cao, Y. Li, X. Zhang, and Y. Zou, “Theoretical study of tunable chirality from graphene integrated achiral metasurfaces,” Photon. Res. Vol. 5, pp. 441-449, 2017.

[37] J. Zhao, J. Zhang, Z. Zhu, X. Yuan, and S. Qin, “Tunable asymmetric transmission of THz wave through a graphene chiral metasurface,” J. Opt. Vol. 18, pp. 095001 (1-5), 2016.

[38] Y. Huang, Z. Yao, F. Hu, C. Liu, L. Yu, Y. Jin, and X. Xu, “Tunable circular polarization conversion and asymmetric transmission of planar chiral graphene-metamaterial in terahertz region,” Carbon, Vol. 119, pp. 305-313, 2017.

[39] Robert Schreiber, N. Luong, Z. Fan, A. Kuzyk, P. C. Nickels, T. Zhang, D. M. Smith, B. Yurke, and T. Liedl, “Chiral plasmonic DNA nanostructures with switchable circular dichroism,” Nat. Commun. Vol. 4, pp. 2948, 2013.

[40] J. Liu, M. Jalali, S. Mahshida and S. Wachsmann-Hogiu, “Are plasmonic optical biosensors ready for use in point-of-need applications?,” Analyst, Vol. 145, pp. 364-384, 2020.

[41] J. McCall, “Genetic algorithms for modelling and optimisation,” J. Comput. Appl. Maths. Vol. 184, pp. 205–222, 2005.

[42] K. Rouhi, H. Rajabalipanah, and A. Abdolali, “Real-Time and Broadband Terahertz Wave Scattering Manipulation via Polarization-Insensitive Conformal Graphene-Based Coding Metasurfaces,” Ann. Phys. Vol. 530, pp. 1700310 (1-9), 2017.

[43] P. Kumar, A. Lakhtakia, and P. K. Jain, “Graphene-pixel-based polarization-insensitive metasurface for almost perfect and wideband terahertz absorption,” J. Opt. Soc. Am. B, Vol. 36, pp. F84-F88, 2019.

[44] M. J. Chashmi, P. Rezaei, and N. Kiani, “Polarization controlling of multi resonant graphene-based microstrip antenna,” Plasmonics, 2019.

[45] Z Xu, D. Wu, Y. Liu, C. Liu, Z. Yu, L. Yu, and H. Ye, “Design of a Tunable Ultra-Broadband Terahertz Absorber Based on Multiple Layers of Graphene Ribbons,” Nanoscale Res. Lett. Vol. 13, pp. 1-8, 2018.

[46] A. Andryieuski and A. V. Lavrinenko, “Graphene metamaterials based tunable terahertz absorber: effective surface conductivity approach,” Opt. Express, Vol. 21, pp. 9144-9155.

[47] B. Wang, X. Zhang, X. Yuan, and J. Teng, “Optical coupling of surface plasmons between graphene sheets,” Appl. Phys. Lett. Vol. 100, pp. 131111, 2012.

[48] Y. Liu, R. Zhong, Z. Lian, C. Bu, and S. Liu, “Dynamically tunable band stop filter enabled by the metal-graphene metamaterials,” Sci. Rep. Vol. 8, pp. 2828, 2018.

[49] K. F. Mak, L. Ju, F. Wang, and T. F. Heinz, “Optical spectroscopy of graphene: from the far infrared to the ultraviolet,” Solid State Commun. Vol. 152, pp. 1341–1349, 2012.

[50] A. Vakil and N. Engheta, “Transformation optics using graphene,” Science, Vol. 32, pp. 1291–1294, 2011.

[51] A. Fardoost, F. Ghaedi Vanani, A. Amirhoseini, and R. Safian, “Design of Multi-Layer Graphene Based Ultra-Wideband Terahertz Absorber,” IEEE Trans. Nanotechnol. Vol. 16, pp. 68-74, 2017.

[52] Z. Xu, D. Wu, Y. Liu, C. Liu, Z. Yu, L. Yu, and H. Ye, “Design of a Tunable Ultra-Broadband Terahertz Absorber Based on Multiple Layers of Graphene Ribbons,” Nanoscale Res. Lett. Vol. 13, pp. 143 (1-8), 2018.

[53] L. Ren, Q. Zhang, J. Yao, Z. Sun, R. Kaneko, Z. Yan, S. Nanot, Z. Jin, I. Kawayama, M. Tonouchi, J. M. Tour, and J. Kono, “Terahertz and infrared spectroscopy of gated large-area graphene,” Nano Lett. Vol. 12, pp. 3711, 2012.

[54] F. Wang, Y. Zhang, C. Tian, C. Girit, A. Zettl, M. Crommie, and Y. R. Shen, “Gate-Variable Optical Transitions in Graphene,” Science, Vol. 320, pp. 206–209, 2008.

[55] B. Sun and Y. Yu, “Analysis of circular dichroism in chiral metamaterial at terahertz frequencies,” J. Phys. D: Appl. Phys. Vol. 52, pp. 025105 (1-14), 2018.

[56] Y. Qu, L. Huang, L. Wang, and Z. Zhang, “Giant circular dichroism induced by tunable resonance in twisted Z-shaped nanostructure,” Opt. Express, Vol. 25, pp. 5480-5487.

[57] D. Zarifi, M. Soleimani, and V. Nayyeri, “A Novel Dual-band chiral metamaterial structure with giant optical activity and negative refractive index,” J. Electromagn. Waves Appl. Vol. 26, pp. 251–263, 2012.

[58] H.-J. Li, L-L Wang, B. Sun, Z-R. Huang, and X. Zhai, “Tunable mid-infrared plasmonic band-pass filter based on a single graphene sheet with cavities,” J. Appl. Phys. Vol. 116, pp. 224505, 2014.

[59] W. Su, “A four-port ultra-compact terahertz splitting filter based on graphene nanoribbon,” IEEE Photonics Technol. Lett. Vol. 31, pp. 86–89, 2019.

[60] K. Yang, N. Chopra, Q. H. Abbasi, K. Qaraqe, and A. Alomainy, “Collagen Analysis at Terahertz Band using Double-Debye Parameter Extraction and Particle Swarm Optimisation,” IEEE Access, Vol. 14, pp. 1-6, 2015.

[61] Y. Li, X. Chen, F. Hu, D. Li, H. Teng, Q. Rong, W. Zhang, J. Han, and H. Liang, “Four resonators based high sensitive terahertz metamaterial biosensor used for measuring concentration of protein,” J. Phys. D: Appl. Phys. Vol. 52, pp. 118077, 2019.

[62] R. Mendis, V. Astley, J. Liu, and D. M. Mittleman, “Terahertz microfluidic sensor based on a parallel-plate waveguide resonant cavity,” Appl. Phys. Lett. Vol. 95, pp. 171113, 2009.

[63] R. Singh, W. Cao, I. Al-Naib, and L. Cong, W. Withayachumnankul, and W. Zhang, “Ultrasensitive terahertz sensing with high-Q Fano resonances in metasurfaces,” Appl. Phys. Lett. Vol. 105, pp. 171101, 2014.

[64] Y. Wang, W. Cheng, J. Qin, and Z. Han, “Terahertz refractive index sensor based on the guided resonance in a photonic crystal slab,” Opt. Commun. Vol. 434 pp. 163-166, 2019.

[65] I. J. López, P. R. Ulibarri, S. A. Kuznetsov, C. Quemada, and M. Beruete, “Labyrinth Metasurface for Biosensing Applications: Numerical Study on the New Paradigm of Metageometries,” Sensors, Vol. 19 pp. 4396, 2019.

[66] D. Wu, J. Liu, H. Han, Z. Han, and Z. Hong Z, “A high Q terahertz asymmetrically coupled resonator and its sensing performance,” Front. Optoelectron. Vol. 8, pp. 68-72, 2015.

[67] M. M. Keshavarz and A. Alighanbari, “Terahertz refractive index sensor based on Tamm plasmon-polaritons with graphene,” Appl. Opt. Vol. 58, pp. 3604-3612, 2019.

[68] M. S. Islam, J. Sultana, M. Biabanifard, Z. Vafapour, M. J. Nine, A. Dinovitser, C. M. B. Cordeiro, B. W. -H. Ng, and D. Abbott, “Tunable localized surface plasmon graphene metasurface for multiband superabsorption and terahertz sensing,” Carbon, Vol. 158, pp. 559-567, 2020.

[69] Y. Tieshan, L. Han, and J. Baohua, “Two-dimensional material functional devices enabled by direct laser fabrication,” Frontiers of Optoelectronics Vol. 11, pp. 2-22, 2018.

[70] Z. Lu, L. Ma, J. Tan, H. Wang, and X. Ding, “Transparent multi-layer graphene/polyethylene terephthalate structures with excellent microwave absorption and electromagnetic interference shielding performance,” Nanoscale Vol. 8, pp. 16684-16693, 2016.